On the role of multiples in Marchenko imaging

Wapenaar, Kees; van der Neut, Joost; Slob, Evert

Important note
To cite this publication, please use the final published version (if applicable).
Please check the document version above.

On the role of multiples in Marchenko imaging

Kees Wapenaar[1], Joost van der Neut[1], and Evert Slob[1]

ABSTRACT

Marchenko imaging can produce seismic reflection images in which artifacts related to multiples are suppressed. However, in state-of-the-art implementations, multiples do not contribute to the imaged reflectors. With an "event-by-event" deconvolution imaging approach, it is possible to use multiples in Marchenko imaging. We illustrate this for a 1D reflection response in which the primary reflection of a specific interface is missing.

INTRODUCTION

Marchenko imaging (Broggini and Snieder, 2012; Slob et al., 2014; Wapenaar et al., 2014) is a novel seismic imaging technique that has the potential to produce seismic reflection images, free of artifacts related to internal multiples (Broggini et al., 2014; van der Neut et al., 2015; Ravasi et al., 2016) and surface-related multiples (Singh et al., 2017). An intriguing question is whether the multiples are only eliminated or whether they also contribute to the imaged reflectors. In this paper, we show that (1) multiples are eliminated in the current implementation of Marchenko deconvolution imaging and (2) multiples may contribute to the image in a modified implementation. Instead of proving this rigorously, we have chosen to illustrate both aspects with simple 1D examples. We hope that these examples will stimulate further research toward the use of multiples in 2D and 3D Marchenko imaging schemes.

GREEN'S FUNCTION RETRIEVAL WITH THE MARCHENKO METHOD

For an acoustic, horizontally layered lossless medium, the basic expressions underlying Green's function retrieval with the Marchenko method are the following two Green's function representations:

$$G^-(z_A, z_0, t) + f_1^-(z_0, z_A, t)$$
$$= \int R(z_0, t - t') f_1^+(z_0, z_A, t') dt', \qquad (1)$$

and

$$G^+(z_A, z_0, t) - f_1^+(z_0, z_A, -t)$$
$$= -\int R(z_0, t - t') f_1^-(z_0, z_A, -t') dt'. \qquad (2)$$

Here, $G^+(z_A, z_0, t)$ and $G^-(z_A, z_0, t)$ are the downgoing (+) and upgoing (−) parts at depth z_A of Green's function $G(z_A, z_0, t)$, which is the response to an impulsive plane-wave source at the upper boundary z_0, as a function of time t. We assume that the positive z-axis points downward; hence, $z_A > z_0$. The function $R(z_0, t)$ is the impulsive reflection response at z_0 of the layered medium and $f_1^+(z_0, z_A, t)$ and $f_1^-(z_0, z_A, t)$ are the down- and upgoing parts at z_0 of the focusing function $f_1(z_0, z_A, t)$. Although $G(z_A, z_0, t)$ and $R(z_0, t)$ are defined in the actual medium (which is bounded by a homogeneous half-space above z_0), the focusing function is defined in a reference medium, which is identical to the actual medium above z_A and homogeneous below z_A. By definition, it collapses to a delta function at the focal depth z_A; hence, $f_1(z_A, z_A, t) = \delta(t)$ (Slob et al., 2014).

Let t_d denote the time of the direct arrival in $G(z_A, z_0, t)$. We define a time-window function $w(t) = H(t_d - \epsilon - t)$, where $H(t)$ is the Heaviside step function and ϵ is a small positive constant. By multiplying the left and right sides of equations 1 and 2 by $w(t)$, Green's functions are suppressed, leaving two equations for the two unknowns $f_1^+(z_0, z_A, t)$ and $f_1^-(z_0, z_A, t)$. Assuming that the reflection response $R(z_0, t)$ is known (from measurements), these equations can be solved iteratively, starting with an initial estimate $f_{1,0}^+(z_0, z_A, t)$, defined as the inverse of the direct arrival of $G(z_A, z_0, t)$. This initial estimate is often simplified as $f_{1,0}^+(z_0, z_A, t) = \delta(t + t_d)$ (Rose, 2002). Once the focusing functions are found, they are substituted into original equations 1 and 2, yielding Green's functions

$G^+(z_A, z_0, t)$ and $G^-(z_A, z_0, t)$. For more details (also for the 2D and 3D versions), see the references mentioned in the "Introduction" section.

We illustrate this for a horizontally layered medium, consisting of four layers, enclosed between two homogeneous half-spaces. The propagation velocities of the four layers are $c_1 = 2000$, $c_2 = 4000$, $c_3 = 2000$, and $c_4 = 4000$, all expressed in meters per second, and the mass densities are $\rho_1 = 1000$, $\rho_2 = 2000$, $\rho_3 = 1000$, and $\rho_4 = 2000$, expressed in kilograms per cubic meter. The depths of the layer boundaries are $z_0 = 0$, $z_1 = 400$, $z_2 = 850$, $z_3 = 1450$, and $z_4 = 2200$, all expressed in meters. The half-spaces above z_0 and below z_4 have a propagation velocity of 2000 m/s and a mass density of 1000 kg/m^3. The reflection coefficients of the four interfaces are $r_1 = 0.6$, $r_2 = -0.6$, $r_3 = 0.6$, and $r_4 = -0.6$. The reflection response $R(z_0, t)$ is numerically modeled using the reflectivity method (Kennett, 1983).

We apply the procedure outlined above for a range of z_A values (which we call z when it is treated as a variable), from 25 to 2300 m, with steps of 25 m. Our input is $R(z_0, t) * s(t)$, where $*$ denotes convolution and $s(t)$ is a Ricker wavelet with a central frequency of 50 Hz. Figure 1 shows the retrieved Green's function $G(z, z_0, t) * s(t) = \{G^+(z, z_0, t) + G^-(z, z_0, t)\} * s(t)$, displayed as a function of depth and time (such as in a vertical seismic profile [VSP]). To enhance the multiples in this display, each trace has been multiplied by $\exp\{\alpha(t - t_d(z))\}$, with $\alpha = 1.2$. Note that, apart from the reflection response $R(z_0, t) * s(t)$, the only information used to arrive at the result of Figure 1 is $t_d(z)$, the time of the direct arrival. This requires that an estimate of the velocity model is available

(a smooth model is sufficient). If the depth axis would be replaced by t_d, then no velocity model whatsoever would be required.

COMPARISON OF IMAGING CONDITIONS

Given the down- and upgoing fields as a function of space and time (such as in Figure 1), several approaches in imaging are possible. We analyze deconvolution and correlation imaging approaches that are currently being used in Marchenko imaging. Other imaging approaches, such as least-squares imaging (Nemeth et al., 1999) and nonlinear scattering-based imaging (Fleury and Vasconcelos, 2012), are beyond the scope of this analysis.

Marchenko deconvolution imaging

At a given depth level z_A, the down- and upgoing Green's functions are mutually related via

$$G^-(z_A, z_0, t) = \int R(z_A, t - t') G^+(z_A, z_0, t') dt'. \quad (3)$$

Here $R(z_A, t)$, for $z_A > z_0$, is the impulsive reflection response at z_A of the layered medium below z_A, assuming a homogeneous half-space above z_A. The function $R(z_A, t)$ can be resolved from equation 3 by deconvolution, thus representing the redatumed reflection response. An image is obtained by convolving the redatumed response with the original wavelet and selecting the $t = 0$ component at each depth; hence, $[R(z, t) * s(t)]_{t=0}$. The result is shown in Figure 2a, as a function of variable depth z (for a larger depth range than shown in Figure 1). Because the redatumed responses have been obtained by deconvolution, we call this the Marchenko deconvolution image. Note that the reflection coefficients of ± 0.6 are perfectly recovered and no artifacts related to the multiple reflections are present. For comparison, Figure 2b shows the standard imaging result (correlation of down- and upgoing waves obtained by one-way wavefield extrapolation, without any correction for multiple reflections).
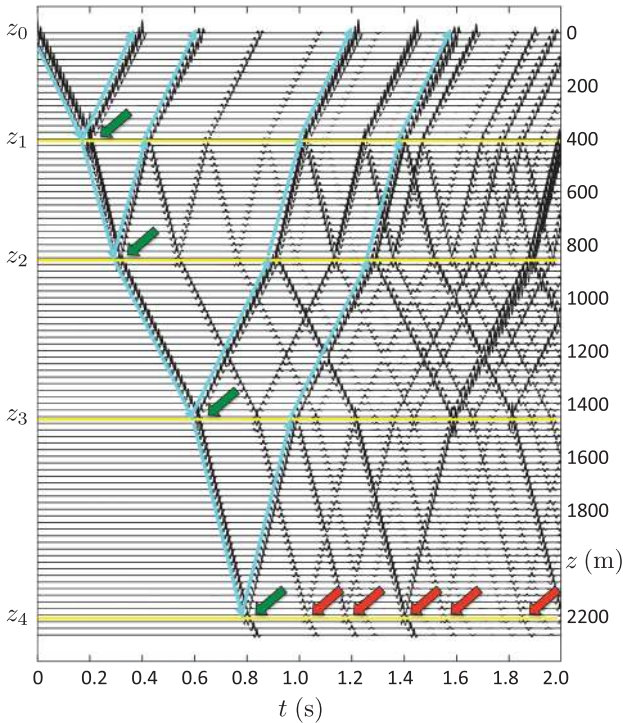

Figure 1. Retrieved Green's function $G(z, z_0, t) * s(t)$. The imaged reflectors in Figure 2a come from the first arrivals in the down- and upgoing Green's functions just above these reflectors, indicated by the green arrows.
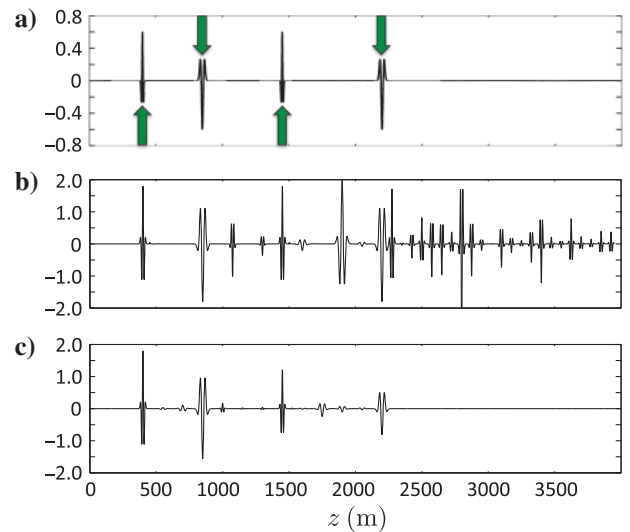

Figure 2. (a) Marchenko deconvolution image. (b) Standard correlation image. (c) Marchenko correlation image.

We now analyze how the image of the fourth reflector in Figure 2a has been obtained. For simplicity, we ignore the effect of the wavelet $s(t)$ in this analysis. Just above the fourth reflector, the reflection response is given by $R(z_4^\epsilon, t) = r_4 \delta(t)$, with $z_4^\epsilon = z_4 - \epsilon$. This is the desired outcome of the deconvolution process. Let us write the downgoing Green's function just above the reflector as

$$G^+(z_4^\epsilon, z_0, t) = a\delta(t - t_{\mathrm{d}}) + M_1(t - t_{\mathrm{d}}), \qquad (4)$$

where the delta function denotes the direct arrival (a being its amplitude) and the second term represents a coda $M_1(t)$, delayed by t_{d}. The coda is causal; i.e., $M_1(t) = 0$ for $t \leq 0$. For the upgoing Green's function just above this reflector, we write

$$G^-(z_4^\epsilon, z_0, t) = r_4 a\delta(t - t_{\mathrm{d}}) + r_4 M_1(t - t_{\mathrm{d}}). \qquad (5)$$

The direct arrivals in G^+ and G^- are indicated by the deepest green arrow in Figure 1, and the codas are indicated by the red arrows. Looking at the simple relation between the down- and upgoing Green's functions (equations 4 and 5), one could intuitively expect that, by deconvolving G^- for G^+, the first arrival and the coda would contribute to the retrieval of the reflection coefficient r_4. However, we show that only the first arrival contributes.

To resolve $R(z_4^\epsilon, t)$ from Green's functions, we invert equation 3, according to

$$R(z_4^\epsilon, t) = \int G^-(z_4^\epsilon, z_0, t - t') G_{\mathrm{inv}}^+(z_4^\epsilon, z_0, t') \mathrm{d}t', \qquad (6)$$

where $G_{\mathrm{inv}}^+(z_4^\epsilon, z_0, t)$ is the inverse of $G^+(z_4^\epsilon, z_0, t)$. Note that $G^+(z_4^\epsilon, z_0, t)$ is (apart from the transmission coefficient of the last interface) equal to the transmission response of the layered medium; hence, it is a causal minimum-phase signal, delayed by t_{d} (Anstey and O'Doherty, 1971; Robinson and Treitel, 1976). The inverse of a minimum-phase signal is causal and minimum phase as well (Robinson, 1954; Berkhout, 1974); hence, $G_{\mathrm{inv}}^+(z_4^\epsilon, z_0, t)$ is a causal signal, advanced by t_{d}. We write this inverse as

$$G_{\mathrm{inv}}^+(z_4^\epsilon, z_0, t) = a^{-1}\delta(t + t_{\mathrm{d}}) + M_2(t + t_{\mathrm{d}}), \qquad (7)$$

with the causal coda $M_2(t)$ obeying $M_2(t) = 0$ for $t \leq 0$. Substituting equations 5 and 7 into equation 6 gives

$$R(z_4^\epsilon, t) = r_4 \delta(t) + (r_4/a) M_1(t) + r_4 a M_2(t)$$
$$+ r_4 \int M_1(t - t'') M_2(t'') \mathrm{d}t'', \qquad (8)$$

with $t'' = t' + t_{\mathrm{d}}$. Note that the first term on the right side (which comes from the first arrivals) is the desired outcome; hence, the other three terms by definition compensate each other. What is more important is that these three terms are all causal; hence, none of these terms contributes to the result at $t = 0$. In other words, the result at $t = 0$ (responsible for the image of r_4) comes entirely from the first arrivals in the down- and upgoing Green's functions at z_4^ϵ, indicated by the deepest green arrow in Figure 1. Because $G^+(z, z_0, t)$ for arbitrary $z > z_0$ can be written as a convolution of two minimum-phase functions (Wapenaar et al. [2013], equation 7), its inverse is causal (advanced by $t_{\mathrm{d}}(z)$); hence, the same reasoning as above also holds for the images of the other reflectors

(indicated by the other green arrows in Figure 1). Finally, using the fact that the coda of the focusing function is causal, it can be shown in a similar way that the first arrival in $G^-(z_n^\epsilon, z_0, t)$ ($n = 1, 2, 3, 4$) comes, in turn (via equation 1), from the primary reflection of the nth reflector, i.e., $R(z_0, 2t_{\mathrm{d}}(z_n))$. Hence, the imaged reflectors in Figure 2a come from the primary reflections in the reflection response $R(z_0, t)$.

This somewhat counterintuitive conclusion is one of the main results of this paper. Note that, although the multiples in $R(z_0, t)$ do not contribute to the imaged reflectors, they played an essential role in obtaining the correct Green's functions in Figure 1 and hence in the suppression of artifacts such as those in Figure 2b.

Marchenko correlation imaging

Consider again Figure 1, in which the red arrows indicate the codas in G^+ and G^- just above the fourth reflector. Because the down- and upgoing codas are time coincident just above this reflector (similar to the direct waves), it is expected that they contribute in Marchenko correlation imaging (Behura et al., 2014). We show that this is indeed the case. We define the correlation of the down- and upgoing fields as follows:

$$\hat{R}(z_4^\epsilon, t) = \int G^-(z_4^\epsilon, z_0, t - t') G^+(z_4^\epsilon, z_0, -t') \mathrm{d}t', \qquad (9)$$

where $\hat{R}$ denotes an estimate of R. Note that, in comparison with equation 6, the time-advanced causal function $G_{\mathrm{inv}}^+(z_4^\epsilon, z_0, t')$ has been replaced by the time-advanced acausal function $G^+(z_4^\epsilon, z_0, -t')$. This makes a difference when it comes to the contribution of multiples to the image. Substitution of equations 4 and 5 into equation 9 gives

$$\hat{R}(z_4^\epsilon, t) = r_4 a^2 \delta(t) + r_4 a\{M_1(t) + M_1(-t)\}$$
$$+ r_4 \int M_1(t - t'') M_1(-t'') \mathrm{d}t''. \qquad (10)$$

This time, the first and last terms contribute to the result at $t = 0$, the last term being the autocorrelation of the coda. Hence, in this case, the multiples in the data may contribute to improving the signal-to-noise ratio of the image. However, the reflector is imaged with an erroneous amplitude. Moreover, at other depth levels, artifacts occur due to the correlation process (see Figure 2c). Nevertheless, the result is significantly better than the standard imaging result of Figure 2b.

Marchenko event-by-event deconvolution imaging

To improve the amplitudes, the correlation can be replaced by an event-by-event deconvolution, followed by a weighted addition (Minato and Ghose, 2016). With a proper selection of events (e.g., the ones indicated by the red arrows in Figure 1), multiples may thus contribute to true-amplitude images of the reflectors. The example in the next section uses event-by-event deconvolution in a situation in which the other discussed methods break down.

GREEN'S FUNCTION RETRIEVAL AND IMAGING IN THE CASE OF A MISSING PRIMARY

Imaging schemes that use multiples, rather than eliminate them, are particularly relevant when specific reflectors are not illuminated by the primaries (Zhang and Schuster, 2014; Davydenko and

Verschuur, 2015). In a 1D experiment, this situation does not occur. Here, we discuss an example of Green's function retrieval and imaging in the case of a missing primary reflection. Our aim is not to present a general approach, but merely to illustrate that the Marchenko method can still lead to a useful result when a primary reflection is missing (or hidden by a noise burst), by using information in a carefully selected multiply reflected event.

We remove the primary reflection of the third interface at $t = 2t_d(z_3)$ from the reflection response $R(z_0, t) * s(t)$. First, we apply the Green's function retrieval scheme discussed above without any modification. Hence, we use the windowed versions of equations 1 and 2 to estimate the focusing functions $f_1^+(z_0, z_A, t)$ and $f_1^-(z_0, z_A, t)$. Because these functions and their time reversals reside in the finite time window $-t_d(z_A) \leq t \leq t_d(z_A)$, the reflection function $R(z_0, t)$ in the windowed version of equations 1 and 2 is only "probed" in the interval $0 < t < 2t_d(z_A)$. Hence, as long as $z_A < z_3$, the missing primary at $t = 2t_d(z_3)$ has no effect on the estimation of the focusing functions; only for $z_A \geq z_3$ are the retrieved focusing functions no longer correct. Next, the retrieved focusing functions are used in original equations 1 and 2 to obtain the down- and upgoing Green's functions. The result is shown in Figure 3. Because of the finite support of the focusing functions, the missing primary at $t = 2t_d(z_3)$ affects the results of the integrals in equations 1 and 2 only in the time window $2t_d(z_3) - t_d(z) \leq t \leq 2t_d(z_3) + t_d(z)$ (where z stands again for the variable z_A). This "cone of influence" is indicated by the light-green shaded area between z_0 and z_3 (below z_3, the focusing functions are not correct, hence, we restrict this analysis to the

region above z_3). Outside this cone, the result in Figure 3 is identical to that in Figure 1. This does not imply that everything inside the cone is affected by the missing primary. From a more detailed analysis of the focusing function, it follows that above z_3, only the dark-green shaded area (the "thick rays") in Figure 3 is influenced by the missing primary.

For the imaging step, we use an event-by-event deconvolution approach. First, we deconvolve the upgoing field in Figure 3 for the downgoing first arrival at all depths. The result is shown in Figure 4a. The green arrows indicate the imaged first, second, and fourth reflectors; the yellow arrow indicates an artifact inside the fourth layer; and the red arrow indicates the position of the missing image of the third reflector. Furthermore, note the many artifacts below the fourth reflector. An advantage of the VSP-like display in Figure 3 is that the paths of primary and multiple reflections can be followed through the medium. The red rays in this figure indicate a multiple that illuminates the third reflector, inside the light-green cone, but outside the dark-green area that is affected by the missing primary. We select the down- and upgoing events associated with this multiple in layer 3, and we use these for deconvolution imaging in layer 3, yielding the image of the third reflector, indicated by the red arrow in Figure 4b. Note that, similar to Figure 2a, the first three layers are now perfectly imaged. Below the third reflector, the scheme is no longer reliable because the retrieved focusing functions are incomplete.

Now that the third reflector has been imaged via a multiple refection, its primary response is modeled. The imaged reflection coefficients r_1 and r_2 are used to compute the transmission loss of the medium above this reflector. This primary response is added to the reflection data at $t = 2t_d(z_3)$. Next, the original Marchenko scheme is continued to also correctly image below the restored reflector (see Figure 4c).

It should be noted that this numerical experiment has been carried out under idealized conditions. We considered a purely 1D acoustic situation, all events were distinguishable in time, and the response
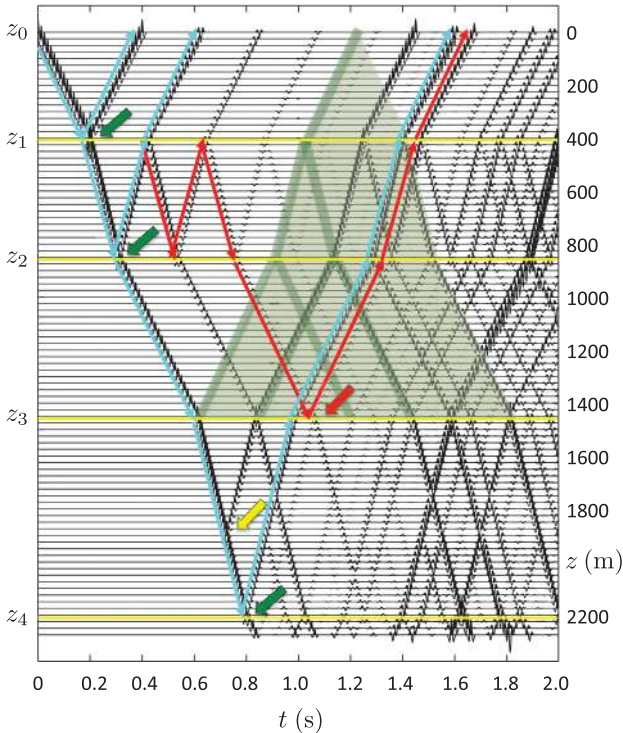

Figure 3. As Figure 1, after removal of the primary of the third reflector. The imaged reflectors in Figure 4b come from the down- and upgoing waves above these reflectors, indicated by the green and red arrows. The yellow arrow indicates the origin of the artifact inside the fourth layer in Figure 4a and 4b.
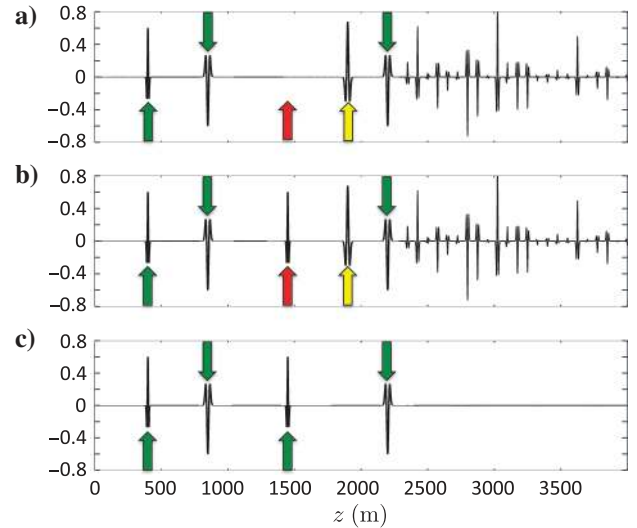

Figure 4. Marchenko event-by-event deconvolution images obtained from the reflection response, which misses the primary of the third reflector. (a) Image obtained from the primaries. (b) The same, but including the image of the third reflector, obtained from the multiple indicated by the red rays in Figure 3. (c) Image obtained after restoration of the primary response of the third reflector.

was noise free. Moreover, we assumed that it is known beforehand that the primary response of the third reflector is missing.

CONCLUSION

We have shown that with the state-of-the-art implementation of Marchenko deconvolution imaging, although artifacts related to multiples are eliminated from the image, multiples do not contribute to the imaged reflectors. We have also shown that with an event-by-event deconvolution approach, it is in principle possible to use multiples in Marchenko imaging, even when the primary reflection is missing.

This paper provides only a start of research toward the use of multiples in Marchenko imaging. Further research will include the development of methods to identify primaries and multiples in the retrieved Green's functions, the extension to 2D and 3D situations and the extension to the elastodynamic situation.

ACKNOWLEDGMENTS

REFERENCES

Anstey, N. A., and R. F. O'Doherty, 1971, Reflections on amplitudes: Geophysical Prospecting, **19**, 430–458, doi: 10.1111/j.1365-2478.1971.tb00610.x.

Behura, J., K. Wapenaar, and R. Snieder, 2014, Autofocus imaging: Image reconstruction based on inverse scattering theory: Geophysics, **79**, no. 3, A19–A26, doi: 10.1190/geo2013-0398.1.

Berkhout, A. J., 1974, Related properties of minimum-phase and zero-phase time functions: Geophysical Prospecting, **22**, 683–709, doi: 10.1111/j.1365-2478.1974.tb00111.x.

Broggini, F., and R. Snieder, 2012, Connection of scattering principles: A visual and mathematical tour: European Journal of Physics, **33**, 593–613, doi: 10.1088/0143-0807/33/3/593.

Broggini, F., R. Snieder, and K. Wapenaar, 2014, Data-driven wavefield focusing and imaging with multidimensional deconvolution: Numerical examples for reflection data with internal multiples: Geophysics, **79**, no. 3, WA107–WA115, doi: 10.1190/geo2013-0307.1.

Davydenko, M., D. J. Verschuur, and G. J. A. van Groenestijn, 2015, Full wavefield migration applied to field data: 77th Annual International Conference and Exhibition, EAGE, Extended Abstracts, We-N101-10.

Fleury, C., and I. Vasconcelos, 2012, Imaging condition for nonlinear scattering-based imaging: Estimate of power loss in scattering: Geophysics, **77**, no. 1, S1–S18, doi: 10.1190/geo2011-0135.1.

Kennett, B. L. N., 1983, Seismic wave propagation in stratified media: Cambridge University Press.

Minato, S., and R. Ghose, 2016, Enhanced characterization of fracture compliance heterogeneity using multiple reflections and data-driven Green's function retrieval: Journal of Geophysical Research, **121**, 2813–2836, doi: 10.1002/2015JB012587.

Nemeth, T., C. Wu, and G. Schuster, 1999, Least-squares migration of incomplete reflection data: Geophysics, **64**, 208–221, doi: 10.1190/1.1444517.

Ravasi, M., I. Vasconcelos, A. Kritski, A. Curtis, C. A. da Costa Filho, and G. A. Meles, 2016, Target-oriented Marchenko imaging of a North Sea field: Geophysical Journal International, **205**, 99–104, doi: 10.1093/gji/ggv528.

Robinson, E. A., 1954, Predictive decomposition of seismic traces with applications to seismic exploration: Ph.D. thesis, Massachusetts Institute of Technology.

Robinson, E. A., and S. Treitel, 1976, Net downgoing energy and the resulting minimum-phase property of downgoing waves: Geophysics, **41**, 1394–1396, doi: 10.1190/1.1440689.

Rose, J. H., 2002, 'Single-sided' autofocusing of sound in layered materials: Inverse Problems, **18**, 1923–1934, doi: 10.1088/0266-5611/18/6/329.

Singh, S., R. Snieder, J. van der Neut, J. Thorbecke, E. Slob, and K. Wapenaar, 2017, Accounting for free-surface multiples in Marchenko imaging: Geophysics, **81**, this issue, doi: 10.1190/geo2015-0646.1.

Slob, E., K. Wapenaar, F. Broggini, and R. Snieder, 2014, Seismic reflector imaging using internal multiples with Marchenko-type equations: Geophysics, **79**, no. 2, S63–S76, doi: 10.1190/geo2013-0095.1.

van der Neut, J., K. Wapenaar, J. Thorbecke, E. Slob, and I. Vasconcelos, 2015, An illustration of adaptive Marchenko imaging: The Leading Edge, **34**, 818–822, doi: 10.1190/tle34070818.1.

Wapenaar, K., F. Broggini, E. Slob, and R. Snieder, 2013, Three-dimensional single-sided Marchenko inverse scattering, data-driven focusing, Green's function retrieval, and their mutual relations: Physical Review Letters, **110**, 084301, doi: 10.1103/PhysRevLett.110.084301.

Wapenaar, K., J. Thorbecke, J. van der Neut, F. Broggini, E. Slob, and R. Snieder, 2014, Marchenko imaging: Geophysics, **79**, no. 3, WA39–WA57, doi: 10.1190/geo2013-0302.1.

Zhang, D., and G. T. Schuster, 2014, Least-squares reverse time migration of multiples: Geophysics, **79**, no. 1, S11–S21, doi: 10.1190/geo2013-0156.1.